Advances in Aircraft and Spacecraft Science, *Vol. 9, No. 2 (2022) 131-148*
https://doi.org/10.12989/aas.2022.9.2.131

CFD Simulation of NACA 2412 airfoil with new cavity shapes

Samuel Merryisha[1a], Parvathy Rajendran[*1,2] and Sher Afghan Khan[3b]

[1]School of Aerospace Engineering, Universiti Sains Malaysia, Engineering Campus, Nibong Tebal 14300, Pulau Pinang, Malaysia
[2]Faculty of Engineering & Computing, First City University College, Bandar Utama, Petaling Jaya 47800, Selangor, Malaysia
[3]Department of Mechanical Engineering, Faculty of Engineering, International Islamic University, Kuala Lumpur 53100, Selangor, Malaysia

(Received September 8, 2021, Revised January 25, 2022, Accepted February 7, 2022)

Abstract. The paper presents the surface-modified NACA 2412 airfoil performance with variable cavity characteristics such as size, shape and orientation, by numerically investigated with the pre-validation study. The study attempts to improve the airfoil aerodynamic performance at 30 m/s with a variable angle of attack (AOA) ranging from 0° to 20° under Reynolds number (R_e) 4.4×10^5. Through passive surface control techniques, a boundary layer control strategy has been enhanced to improve flow performance. An intense background survey has been carried out over the modifier orientation, shape, and numbers to differentiate the sub-critical and post-critical flow regimes. The wall-bounded flows along with its governing equations are investigated using Reynolds Average Navier Strokes (RANS) solver coupled with one-equational transport Spalart Allmaras model. It was observed that the aerodynamic efficiency of cavity airfoil had been improved by enhancing maximum lift to drag ratio ((*l/d*) max) with delayed flow separation by keeping the flow attached beyond 0.25C even at a higher angle of attack. Detailed investigation on the cavity distribution pattern reveals that cavity depth and width are essential in degrading the early flow separation characteristics. In this study, overall general performance comparison, all the cavity airfoil models have delayed stalling compared to the original airfoil.

Keywords: aerodynamic performance; cavity; CFD simulation; flow separation; surface modifier; surface roughness; variable orientation

1. Introduction

The military application focuses on short-distance take-off and landing, requiring a multi-elemental wing as a flow control device. However, this multi-tasking has a high level of complexity due to massive retractable systems. The aerodynamic design is expected and pursued in flying vehicles and most transport sources to minimise drag. A recent attractive approach towards aerodynamically improved design is through surface flow control techniques, streamed into two classes (Dandan *et al.* 2019, Merryisha and Parvathy 2019). The active technique involves a higher

*Corresponding author, Ph.D., E-mail: aeparvathy@usm.my
[a]Ph.D. Student, E-mail: merryishagracia@gmail.com
[b]Ph.D., E-mail: sakhan06@gmail.com

http://www.techno-press.org/?journal=aas&subpage=7 ISSN: 2287-528X (Print), 2287-5271 (Online)

jet injection, electric arc energiser, and suction of low-velocity flow to energise the boundary layer and keep the high-velocity flow attached to the surface. These active techniques need higher maintenance of sub-systems and qualified handling techniques. In addition, they are more complicated due to the retractable system functions and axes of flight, thus creating a stronger adverse pressure gradient due to overloading. The passive technique has attracted the researcher's interest due to its compatibility in maintenance and installation (Afzal and Khan 2020). Indenting and protruding the surface generates streamwise vortices, energising the flow and remodifying the adverse pressure gradient region (Afzal and Aabid 2020). Thus, the vortices are stable and small, which counter rotates with the mainstream vortex to depreciate the drag penalty without substantially affecting the lift performance. The separation zone for the surface-modified airfoil is delayed as the vortices overcome the adverse pressure gradient (Lin *et al.* 1992).

Numerous researchers have proposed efficient surface modifier techniques to delay boundary layer separation. All the studies have commonly relieved that creating turbulence before the adverse pressure gradient region to improves flow behaviour. The boundary layer transition has an emerging role in the adverse pressure gradient effect (Merryisha and Rajendran 2019). The concept of indenting cavities over the wing surface has its era from golf ball aerodynamics. The cavity initialises the early transition of the unsteady shear layer, creating laminar separation bubbles and keeps the flow attached to the surface.

The concept of this surface cavities has been enhanced with an aim to improve the airfoil aerodynamic coefficient (lift, drag and lift to drag) with minimal adverse effect along with delaying stalling characteristics. For this purpose, commercial CFD simulation has been conducted over eight different cavity geometries, and their boundary conditions are assigned pre-hand. In order to verify the cavity airfoil performance, validation has been simulated over smooth NACA 2412 airfoil.

2. Background and theory

2.1 Previous studies on passive flow control techniques

Over past decades, researchers show utmost interest in rough surface aerodynamics, giving rise to passive control surface modifiers with golf ball aerodynamics' base concept. Passive surface modifiers generate streamwise vortices that interact with the spanwise vortices from the existing boundary flow; thereby, the vortices strength gets depreciated and thus keeps the flow attached for a longer period. This roughness over the surface creates kinetic energy in the flow, thus energises the boundary layer and keeps the flow re-attached even at lower R_e condition and higher angle of attack (AOA). However, as in lower R_e, a sudden increase in drag and a degrading lift is observed as the AOA increases, mainly due to non-reattachment of separated laminar boundary layer flow (Mueller and DeLaurier 2003). In order to determine the suitable surface modifier, an overview has to be made over variable cavity characteristics and parameters. The general list of existing surface modifiers with their geometric allowances is tabulated in Table 1.

Creating disturbing roughness or patterns over the smooth surface promotes laminar-turbulent transition, which controls laminar flow separation by overcoming the adverse gradients (Feng *et al.* 2015). Thus, the implementation of the cavity has shown promising advantages towards aerodynamic performance improvement and less sensitivity towards mechanical losses.

The optimum aerodynamic characteristics of an airfoil are achieved only when the flow is attached to the surface. As in higher AOA, the airfoil experiences unfavourable dynamic flow

Table 1 Existing surface modifier

Source	Airfoil	Surface model	Roughness shape	Diameter/ width	Height /depth	Spacing		Location
						Stream -wise	Span - wise	
Zhang *et al.* (2018)	-	Flat plate	Semi-spherical cavity with V-rib	4 mm	20 mm	21.6 mm	25 mm	Spread throughout plate
	A circular cavity compounded by v-rib creates down washing vortices due to the complex secondary flow behaviour, thus enhances the local turbulence level resulting in energised kinetic energy in the flow stream.							
D'Alessandro *et al.* (2019)	NACA 642-014	Wing	Semi-spherical cavity	4.7 mm	0.7 C	Spanwise cavity equivalent diameter of 3.35 C.		0.55C
	The cavity effect shows a reduction in laminar separation bubble extension with limited drag and improved lift generation. In addition, the cavities accelerated the flow by controlling the boundary layer scattering keeping it thin and attached for a longer duration.							
Aldheeb *et al.* (2020)	NACA 653218	Wing	Inward porous strip	3 mm	-	Single row inclined at 45°& 90°.		0.90 C
	Porous strip inclined at 90° shows a drastic reduction in the vortex strength, with improved aerodynamic characteristics. The modifier has an advantage of a 67% reduction in tangential velocity and a 212% increase in vortex radius.							
Aldheeb *et al.* (2020)	NACA 653218	Wing	Inward honeycomb structure	5 mm	0.08 mm	Spread out throughout the wingtip		0.90 C
	Honeycomb structure shows a drastic reduction in the vortex strength, with improved aerodynamic characteristics. The modifier has an advantage of a 71% reduction in tangential velocity and a 287% increase in vortex radius.							
Dandan *et al.* (2019)	NACA 2412	Cylinder	Outward semi-spherical cavity	5 mm	2.5 mm	Various half-section & complete cylinder		
	The cavity cylinder shows a massive improvement in drag by 76% reduction compared to a smooth surface and improved lift by keeping the flow attached at a flow velocity of 7.4 m/s.							
Beves and Barber (2017)	Tyrrell 026	Wing	Hemispherical cavity	0.06 C	0.03 C	1.5 D	1.5 D	0.23 C
	The wing surface indented with inward cavities near the leading edge with an endplate of 45×95 mm dimension, 3.5 mm thickness is attached to one end of the wing. The wing with cavities shows the following enhancement - wake size reduction, high velocity under the wing, and reduced wake turbulence.							
Faruqui *et al.* (2014)	NACA 4315	Wing	Semi-spherical bump	-	6.35 mm	Inter-linked		0.8 C
	The bumpy airfoil has improved the delay in flow separation by 6° with improvement in airfoil performance.							
Al-Jibory and Shinan (2020)	NACA 0012	Airfoil	Triangular rib	3.36 mm	3.36 mm	Single rib		0.5 C, 0.7 C, 0.9 C
	Rib placed at 90% of the chord performed better in improving the aerodynamic characteristics up to 14° AOA, beyond which rib located at 50% of chord shows better performance with an improved stall by $+2^\circ$.							
Merryisha and Rajendran (2019)	NACA 2412	Wing	Semi-circular groove	2.3 mm	1.15 mm	0.2C	-	0.2 C, 0.5 C, 0.8 C, all three location
	The presence of groove over the wing has shown at least 0.05% improvement in aerodynamic efficiency compared to the baseline wing, where the triplet groove wing shows the best performance. In addition, the concept of surface grooving has improved stalling by 7.21% and l/d by 9.32%.							

Note: C-Chord, D-Diameter.

characteristics (Chang 1970) with circulating vortex formation generating separation bubbles. The presence of these laminar separation bubbles degrades the aerodynamic performance with increased drag formation. Local separation of flow around the boundary layer creates a slow re-circulation flow region due to the following three factors (Chang 2014, D'Alessandro *et al.* 2019) adverse pressure gradient, separation of the shear layer due to energy losses of turbulent transition and unsteady flow re-attachment.

2.2 Performance of existing cavity models

The low R_e airfoil experiences an abrupt unfavourable stalling with increased drag and a fall in lift coefficient as the AOA increases. Many researchers performed intensive investigations on active and passive surface modifiers to alleviate the negative boundary layer characteristics to improve the stalling and aerodynamic performance. As the active modifiers are more expensive and complicated, passive modifiers are more likely preferred for aerodynamics enhancement for airfoil sustainability. The general aerodynamic performances of the existing cavity models are listed in Table 2. The variable cavity shapes for different airfoil models have been extracted and compared to reveal the cavities' performance at different Mach numbers.

Table 2 Performance evaluation of existing cavity

Source	Airfoil type	Nature of studies	Cavity shape	Mach No.	R_e	AOA range	Best result drawn				
							Max lift (l_{max})	Min drag (d_{min})	Stall angle	Max lift to drag ratio $(l/d)_{max}$	AOA at $(l/d)_{max}$
Livya *et al.* (2015)	NACA 0018	Numerical	Square and compound	0.09 – 0.18	N/A	0° to 20°	0.18	0.05	18°	5.6	14°
Saraf *et al.* (2017)	NACA 0012	Numerical	Semi spherical	0.02	N/A	0° to 16°	1.29	0.241	14°	8.29	10°
Venkatesan *et al.* (2018)	NACA 2412	Experimental	Square	0.09	N/A	0° to 23°	1.15	0.38	16°	N/A	N/A
Ramprasadh and Devanandh (2015)	SELIG 4083	Numerical	Sphere	0.04	N/A	0° to 25°	1.40	0.02	24°	6.04	4°
Chakroun *et al.* (2004)	NACA 0012	Experimental	Groove	0.03	1.5×10^5	0° to 14°	0.9247	0.025	12°	21.45	6°
Wang *et al.* (2015)	NACA 0018	Numerical	Semi ellipsoidal	0.06	3.2×10^5	0° to 20°	0.17	0.03	15°	N/A	N/A
Al-Obaidi and Pei Soh (2016)	NACA 0012	Numerical	Elliptical cavity	0.03	N/A	0° to 10°	0.82	0.022	N/A	18.49	5°

From the researchers' study (Rajasai *et al*. 2015), it is clear that the cavity effect over the airfoil has improved stalling characteristics with improved aerodynamic performance and delayed flow separation. Livya, Anitha *et al*. (2015) studied the comparative performance of NACA 0018 airfoil indented with semi-sphere, square, cylinder, and hexagon-shaped cavity under the working velocity of 30 m/s and 60 m/s with varying AOA 5° to 25°. The improved aerodynamic efficiency is observed more in the inward cavity compared to the outward cavity. Lake *et al*. (2000) study show that the baseline separation occurs between 62% to 78% of the chord length. Hence v-groove indented at

0.6C perform better compared all other groove orientation. His results also present that the suction side modifier shows improved flow behaviour with reduced separation losses.

A similar study has been previously investigated by Srivastav (2012), and his work concluded that both inward and outward cavities show better drag reduction than the smooth airfoil. Saraf *et al*. (2017) investigated the performance of the cavity bumps over NACA 0012 airfoil by varying the cavity placement, and the result declared that cavity placed over 75% of the chord has improved lift by 7%. The same result has been experimentally observed by Arunraj *et al*. (2019) by placing square slots over 40%-75% of NACA 0012 airfoil. The general aerodynamic performance of the existing cavity models is listed in Table 2. The background survey on different types of passive flow control techniques is being carried out in this study, irrespective of three-dimensional or two-dimensional airfoil models, to utilise the modifiers concept as a reference to develop indented and protruded cavities on the NACA 2412 airfoil.

3. Methodology

3.1 Numerical methods and analysis

Over decades the aerodynamic performance of an airfoil at variable boundary conditions has been investigated both experimentally and numerically. However, in recent trends, importance is given towards designing and analysing software as an initial investigation stage for experimental analysis due to its improved compatibility in flow characteristic analysis. Furthermore, CFD methods give a user-friendly platform due to its developed interface capable of solving complex flow field problems.

Von Karman's momentum integral approach Eq. (1) is the simplest two-dimensional boundary layer equation used to solve separations of incompressible flows.

$$\frac{d\theta}{dx} + (2 + H)\frac{\theta}{u_e}\frac{du_e}{dx} = \frac{c_f}{2} = \frac{\tau_w}{\rho U_e^2} \tag{1}$$

Schubauer and Spangenberg (1960) numerically solved the boundary layer mixing Eqs. (2)-(3) through the ratio of momentum thickness (θ) and displacement thickness (δ^*). When the turbulence is inserted into the flow θ remains unchanged as the mixing of flow happens quickly but δ^*depends on $\frac{\partial u}{\partial y}$ as the transition of flow occurs.

$$H = \frac{\delta^*}{\theta} \ , \quad \theta = \int_0^{\propto} \frac{u^{|}}{u_e}\left(1 - \frac{u^{|}}{u_e}\right) dy \tag{2}$$

$$\delta^* = \int_0^{\propto} \left(1 - \frac{u^{|}}{u_e}\right) dy \tag{3}$$

The computational fluid dynamic calculates the forces acting on the fluid elements through Navier-stroke equations and energy conservation equations Eqs. (4)-(6) (Eleni *et al*. 2012); these equations assume the flow to be incompressible and time-dependent when the working regime lies on low Mach number and R_e. The turbulence nature of the flow is determined through Reynold number, R_{cr} terms the flow to be turbulent. These turbulences make the flow unsteady and create a wake at the rear section of the object. The inertial and viscous nature of the flow is governed through

Navier-stroke equations.

$$\frac{\partial u}{\partial x} + \frac{\partial v}{\partial y} = 0 \tag{4}$$

$$u\frac{\partial u}{\partial x} + v\frac{\partial u}{\partial y} = -\frac{1}{\rho}\frac{\partial p}{\partial x} + \frac{\mu}{\rho}\left(\frac{\partial^2 u}{\partial x^2} + \frac{\partial^2 u}{\partial y^2}\right) \tag{5}$$

$$u\frac{\partial v}{\partial x} + v\frac{\partial u}{\partial y} = -\frac{1}{\rho}\frac{\partial p}{\partial y} + \frac{\mu}{\rho}\left(\frac{\partial^2 v}{\partial x^2} + \frac{\partial^2 v}{\partial y^2}\right) \tag{6}$$

RANS turbulence model has been broadly classified into eight different models based on Navier-Stroke argumentation. In this current study, validation has been done over the Spalart Allmaras model (SA), *K-ε* Realisable model, and *K-ω SST* model. As the study is based on low R_e and separated flow behaviour, the SA model provided linear performance to the pre-study results. Moreover, the SA model shows up quite stable approximation results compared to the other two models. The general transport equation for the Spalart Allmaras is as follows in Eq. (7).

$$\frac{\partial \rho\tilde{v}}{\partial t} + \nabla.(\rho\tilde{v}U) = \nabla.\left[(\mu + \rho\tilde{v})\nabla\tilde{v} + C_{b2}\rho\frac{\partial\tilde{v}}{\partial x_k}\frac{\partial\tilde{v}}{\partial x_k}\right] + C_{b1}\rho\tilde{v}\tilde{\Omega} - C_{w1}\rho\left(\frac{\tilde{v}}{ky}\right)^2 f_w \tag{7}$$

Where,

G_v – production of turbulent viscosity

v – molecular kinematic viscosity

ρ – density

$\partial\tilde{v},\ C_{b2}$ - constants

$u_i u_j$ – mean velocity components

$\tilde{v}$ – modified turbulent viscosity

Y_v – destruction of turbulent viscosity

3.2 Description of physical cavity model

The surface modifiers considered in this study are indented and protruded cavities located at different *x/c* locations for each model, as shown in Fig. 1 and Fig. 2. The original airfoil model is tabulated in Table 3. The chord length of the original airfoil (OA) (i.e., smooth baseline airfoil) and cavity airfoil is 230 mm (followed by the validated literature work). Cavities were indented (I) & protruded (P) over the original airfoil with a depth of 1.15 mm, 1.3 mm, a width of 2.3 mm, 4.6 mm and angle tangent the airfoil surface. The depth and width of the cavities are selected based on chord ratios, such as 0.01C, 0.02C for cavity width and 0.005C, 0.006C for cavity depth.

The indented cavity model study consists of 25 different airfoil models with cavities by varying the shape of the cavity and its indented chord location as shown in Fig. 1. The protruded cavity model study consists of 25 different airfoil models with cavities by varying the shape of the cavity

Table 3 NACA 2412 Airfoil Model-1 Original airfoil (OA)

Model	Airfoil model	Specification
Original airfoil (OA)	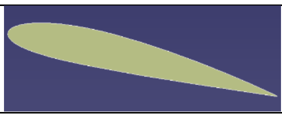	OA airfoil of chord length 230 mm. (Matsson *et al.* 2016)

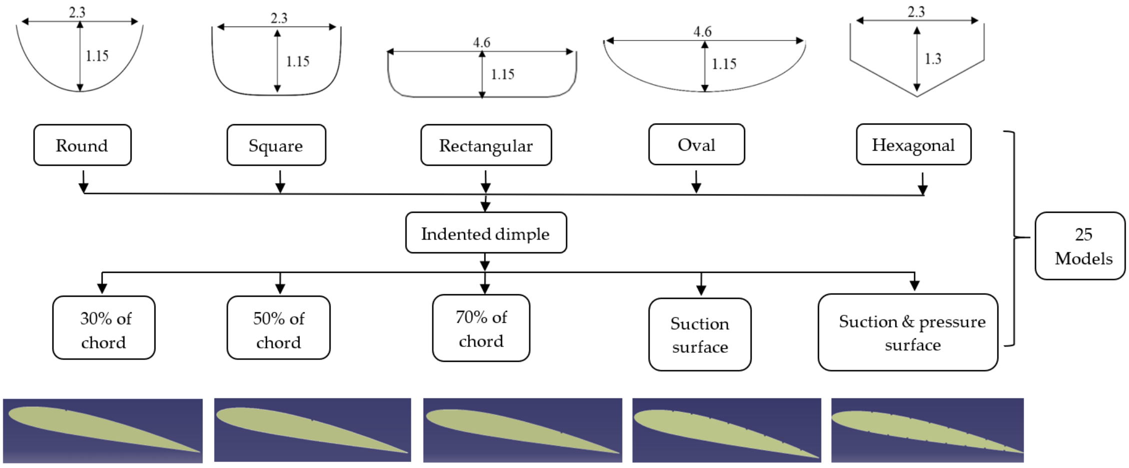

Fig. 1 Indented cavity models

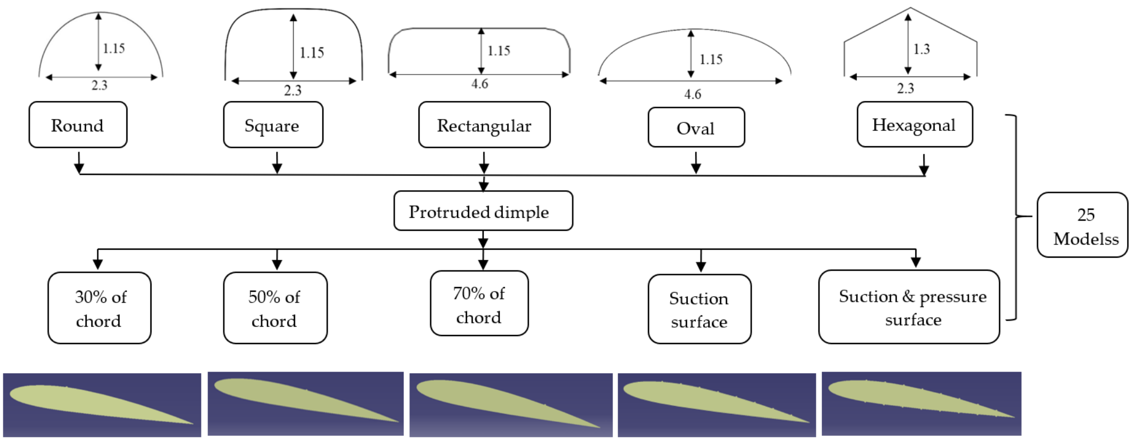

Fig. 2 Protruded cavity models

and its protruded chord location as shown in Fig. 2.

In addition, both indented and protruded models have five different cavity shapes investigated over five different chord locations. The abbreviations of these shapes are as described below.

SRC0.3 - Single Round Cavity at 30%C
SRC0.5 - Single Round Cavity at 50%C
SRC0.7 - Single Round Cavity at 70%C
SSRC - Round Cavity over the suction side of the airfoil
SPRC - Round Cavity over suction and pressure side of the airfoil

SSC0.3 - Single Square Cavity at 30%C
SSC0.5 - Single Square Cavity at 50%C
SSC0.7 - Single Square Cavity at 70%C
SSSC - Square Cavity over the suction side of the airfoil
SPSC - Square Cavity over suction and pressure side of the airfoil

SRcC0.3	- Single Rectangular Cavity at 30%C
SRcC0.5	- Single Rectangular Cavity at 50%C
SRcC0.7	- Single Rectangular Cavity at 70%C
SSRcC	- Rectangular Cavity over the suction side of the airfoil
SPRcC	- Rectangular Cavity over suction and pressure side of the airfoil
SOC0.3	- Single Oval Cavity at 30%C
SOC0.5	- Single Oval Cavity at 50%C
SOC0.7	- Single Oval Cavity at 70%C
SSOC	- Oval Cavity over the suction side of the airfoil
SPOC	- Oval Cavity over suction and pressure side of the airfoil
SHC0.3	- Single Hexagonal Cavity at 30%C
SHC0.5	- Single Hexagonal Cavity at 50%C
SHC0.7	- Single Hexagonal Cavity at 70%C
SSHC	- Hexagonal Cavity over the suction side of the airfoil
SPHC	- Hexagonal Cavity over suction and pressure side of the airfoil

3.3 Domain construction and mesh generation

The partial derivatives of the governing equations are solved through an approximation of finite difference form by defining a definite number of grids throughout the domain boundary. In order to generate accurate results, the closely packed mesh has to define where the grid distribution represents the structural and un-structural meshing quality (Hoffmann and Chiang 2000). Three main factors can improve the quality of the mesh: skewness, orthogonal quality, and wall function (y+), the boundary layer around the airfoil can be made effective through orthogonal gridding (Ramprasadh and Devanandh 2015, Al-Obaidi and Pei Soh 2016). The CFD solutions are very much sensitive to the discretisation of the domain.

The computational meshing has been reformed as follows, structural quadrilateral grid elements are assigned to the outer boundary surface of the domain as of far-field, to predict the diversion of the flow stream, un-structural tetrahedral triangular elements around the airfoil, to elevate the flow divergence around the airfoil surface. These combinations of the irregularity in the meshing eliminated the skewness near the airfoil surface (Manni *et al*. 2016). As stated by Lopes (2016), a huge domain with a far-field boundary of 10 times the chord length is considered in this study, to neglect the effect of the viscous layer on the domain wall boundary and to leave a pathway for flow development both the upstream and downstream of the airfoil. The efficient fine, dense meshing of fine layer $y+\sim 1$ has been incorporated for accurate results with mesh size ranging from 3 to 8 with a total cell of 59,752 (Ramprasadh and Devanandh 2015).

The schematic representation of the C-domain with NACA 2412 airfoil in the mist is shown in Fig. 3. The airfoil is located spanwise (-z) direction inside the domain with horizontally fixed. Finely refined meshing with 320 divisions over suction and pressure of the airfoil has been defined. The growth rate of the grids is in the order of 1.20, extending angular distribution from the airfoil surface (outflow boundary). The performance of the grid growth rate depends upon R_e, chord length, and turbulence modelling. The value of y+ Eq. (8) resolves the turbulence in the flow domain. Adiabatic non-slip condition is given to the airfoil wall, and the remaining boundaries are set to be symmetric boundary conditions. The upper and lower boundaries are assigned to be far-field. The

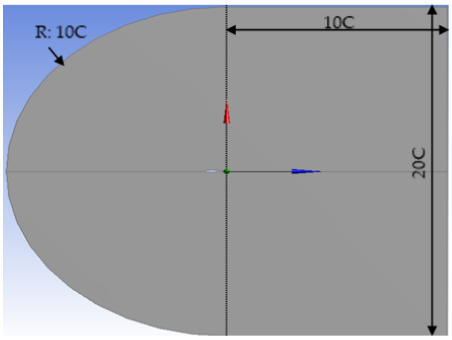

Fig. 3 Projected view of domain with airfoil in the mist

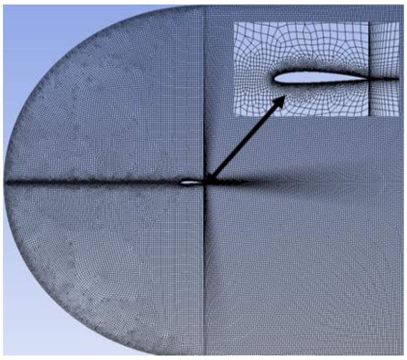

Fig. 4 2D domain grid generation

meshed view is as Fig. 4, and the mesh settings are, Size function-curvature, relevance and span angle centre-fine, maximum face size-20 mm, and growth rate-1.20.

$$y^+ = \frac{u_\tau}{\nu} y_c \text{ , where } u_\tau = \sqrt{\frac{\tau_w}{\rho}} \tag{8}$$

The airfoil wall is finely refined to investigate the flow behaviour and separation by dividing the airfoil surface into 320 sections (Lopes 2016). Adiabatic non-slip condition is applied to the airfoil and walls. Upper and lower boundaries are assigned in the far-field. The mesh settings are, size function: curvature, relevance and span angle centre: fine, maximum face size: 20 mm and growth rate: 1.20.

In this current study, the mesh cell size is refined to be smaller near the airfoil model and increases gradually along the stationary region (domain). The finalised fine mesh and the C-domain gridding and its elevated view of airfoil meshing are shown in Fig. 4. Standard meshing represents a pre-declared basic mesh format where the number of nodes, cells, and faces is lesser with bigger grids. Upon further refinement, the number of elements increases with a high-quality grid and finer mesh. The details of the grid convergence study are tabulated in Table 4.

Table 4 Mesh convergence study

Grid	Cells	Faces	Nodes	α	Cl	Cd
Standard	122645	250809	23057	0°	0.1698	0.0583
				16°	1.0157	0.2895
Coarse	884532	1797369	164522	0°	0.1725	0.0569
				16°	1.1528	0.2830
Medium	1647388	3359024	309708	0°	0.1783	0.0557
				16°	1.2155	0.2801
Fine	2650137	5411579	503526	0°	0.1828	0.0552
				16°	1.2492	0.2792

ANSYS fluent version 18.1 is used as a tool for numerical analysis to determine the performance of two dimensional NACA 2412 airfoil. The simulation is fixed with inlet velocity $u_\infty = 30 \text{ m/s}$

with incorporated R_e=4.4×10^5 and a constant pressure outlet of 1atm has been pre-defined. As the research concept determines the separation of the boundary layer and its wake formation, a huge C-Domain with 10C dimension and C-type meshing topology has been employed. The domain side walls are subjected to non-slip periodic boundary conditions. Turbulence was maintained at 1% to 5% (Lopes 2016) under the RANS model coupled with one equational turbulence model. The following are the working pace given to match the experimental setup for validation on non-slip airfoil walls, as shown in Table 5. The flow type is considered steady-state flow with wall and shear conditions set to stationary and non-slip.

Table 5 Boundary conditions and specifications

Computational parameters / Boundary conditions	Specifications
Cavity surface	Smooth wall
Domain outer boundary	Non-slip wall
Relative specification	Absolute
Inlet boundary type	Velocity inlet
Outlet boundary type	Pressure outlet
Flow velocity	30 m/s
Turbulence kinetic energy	4.184 x 10^{-7} m^{2-}/s^2
Density of air	1.225 Kg/m^3
Dynamic viscosity	1.7894 x 10^{-5} Kg/m-s
Density	1.2043 Kg/m^3
Reference length	0.23m
Gauge pressure	0 pascal
Operating pressure	101325 pascal
Pressure velocity coupling	SIMPLE scheme
Spatial discretisation	First-order upwind

4. Results and discussion

A comparative study has been carried out between the different types of cavity airfoil models and the original airfoil (OA) to determine the effect of cavities on the airfoil surface. The three main variable parameters used in the study are AOA, cavity shape, and orientation.

4.1 Validation

The conceptual model of baseline NACA 2412 airfoil has been compared to the experimental wind tunnel results carried out by Matsson, Voth *et al.* (2016) for validation purposes. The validation study involves a constant working velocity of 30 m/s with variable AOA ranging from 0° to 16° under three different turbulence conditions are, Spalart Allmaras model, *K-ε* Realisable model and *K-ω* SST model.

The results thus obtained shows a good correlation to that of the experimental data. The lift coefficient comparative study declares a 4%-7% error, which shows gradual increment as the AOA increases. There is a maximum noticeable error of 20% in the post-stall regime, and upon validation, the best turbulence model implemented in the cavity airfoil study. In the real-time study, every object has an imaginary turbulence intensity around them, and they lay out no exact theory to predict the relevant turbulence model. These turbulence models can be evaluated through turbulence flow statistics by implementing a simplified constitutive equation. Fig. 5 brings the validation results between the various turbulence model to that of literature results.

The errors thus obtained in Table 6 by the validation study may be due to the nature of flow condition, boundary layer characteristics, and variable RANS model. Therefore, from the validation point of view, the Spalart-Allmaras turbulence model is chosen as the turbulence model for further simulation.

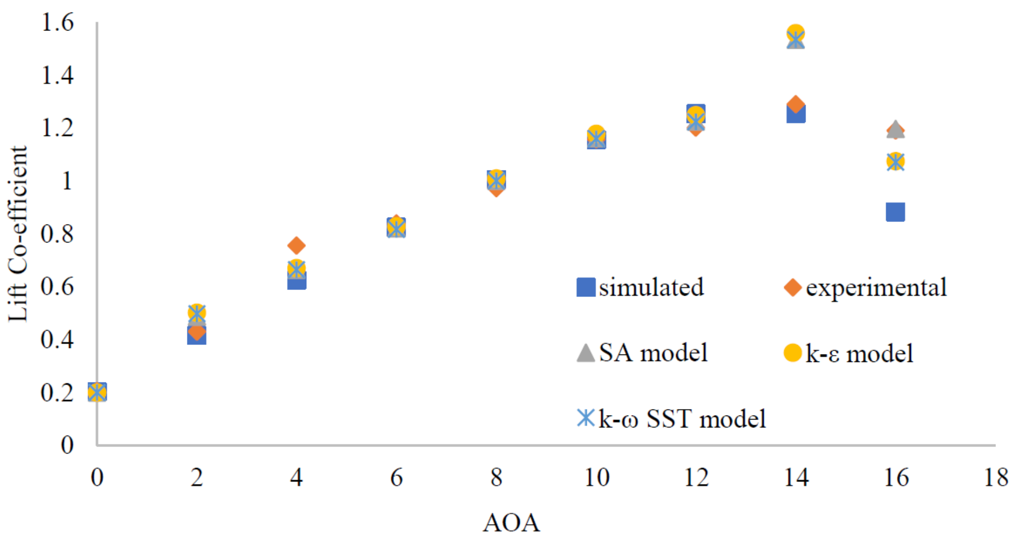

Fig. 5 Validation turbulence model study

Table 6 Average percentage deviation of different turbulence model

% deviation			
Article	SA	*K-ε*	*K-ω* SST
7.17309	6.04011	7.90589	7.38189

4.2 Airfoil models results and performances

The generation of drag is lesser in dimpled airfoil rather than the OA. The generation of drag for the OA is predominant at stalling angles; hence the flow gets separated from the airfoil surface. Different airfoil has their respective advantage towards lift or drag because all the models show inconsistent improvement in both lift and drag. Hence, the lift to drag ratio is evaluated to predict the performance of models suitable for each regime of AOA. Dimpled models show improvement in aerodynamic performance as the AOA increases compared to the OA.

The following conclusions have been drawn for the cavities placed over variable locations:

• Lift coefficient vs AOA: Nine different cavities models located at five different locations have not successfully contributed to lift generation compared to OA. The lift coefficient of cavity airfoil models shows its performance only after the OA stalls.

• Drag coefficient vs AOA: All the nine different cavity airfoil models have shown reduction on drag compared to OA. The maximum drop in drag of different cavity locations to that of AOA compared to OA is discussed in Lift to drag ratio vs AOA: The OA and variant cavity airfoil performance. The performance of specific cavity airfoil models at a certain location has been degraded because of a lack of lift generation. The maximum lift to drag ratio of different cavity locations to that of AOA compared to OA is discussed in Table 7.

• Lift to drag ratio vs AOA: The performance of both the OA and variant cavity airfoil. The performance of specific cavity airfoil models at a certain location has been degraded because of a lack of lift generation. The maximum lift to drag ratio of different cavity locations to that of AOA compared to OA is discussed in Table 7.

As from the output verification, none of the cavity airfoil models has contributed better lift than the original OA regime wise because the lift force is affected by the flow's re-circulation within the cavity. Hence the better coefficient of lift is generated by OA. As discussed in Table 8, cavity airfoil models show outstanding performance in reducing the drag force compared to OA.

Both indented(I) and protruded(P) cavity airfoils have shown reduction in drag. The cavity airfoil models show better performance in improving (l/d) than OA as tabulated in Table 8, even though their performance gets lagged due to the drop in lift performance. The following are the better cavity models based on the regime category.

Regime 1

- o SSHC(I) has reduced drag by 41.8% & SSSC(I) has improved (l/d) by 12.6%
- o SHC(P) 0.5 has reduced drag by 36.9%

Table 7 Aerodynamic performance effect of variable cavity location

Category	Cavity location	0° AOA	4° AOA	8° AOA	12° AOA	16°AOA
% drop in drag of best cavity shape at each AOA	0.3C	SRcC(P): 22.5%	SHC(I): 42.3%	SOC(P): 44%	SOC(I): 31%	SOC(I): 21%
	0.5C	SOC(P): 27%	SOC(I):36%	SOC(I): 35%	SRcC(P): 31%	SOC(P): 23%
	0.7C	SHC(I):20%	SRcC(P): 37%	SHC(P): 43%	SOC(I): 32%	SOC(I): 21%
	Suction side cavities	SSHC(I): 22%	SSHC(I): 42%	SSHC(P): 37%	SSRcC(I): 43%	SSOC(I): 43%
	Suction & pressure side cavities	SPSC(I): 15%	SPSC(I): 24%	SPOC(I): 33%	SPHC(P): 35%	SPRcC(I): 37%
% improvement in l/d of best cavity shape at each AOA	0.3C	SRcC(P): 4.7%	SHC(I): 2%	SOC(P): 11%	SOC(I): 3.7%	SOC(I): 20.3%
	0.5C	-	-	-	SOC(I): 1.5%	SOC(I): 20%
	0.7C	-	SSC(I): 0.4%	SHC(P): 11%	SOC(I): 2.9%	SOC(P): 19.5%
	Suction side cavities	-	SSHC(I): 0.4%	SSSC(I): 4.7%	SSSC(I): 35%	SSSC(I): 56%
	Suction & pressure side cavities	-	-	-	-	SPSC(I): 45%

Note: The table comparison shows until 16° because the original airfoil (OA) stalls at 14°.

Table 8 Aerodynamic performance effect of cavity airfoil models based on regime distribution

Category	Regime	AOA	OA	I/P	Round	Square	Rectangular	Oval	Hexagonal
The best performance of average drag coefficient	1	0°-16°	0.2027	I	-	SPSC: 0.1267	SSR$_C$C: 0.1212	SOC 0.7: 0.1270	**SSHC: 0.1178**
				P	SPRC: 0.1446	SSSC 0.7: 0.1311	SR$_C$C 0.5: 0.1297	SOC 0.5: 0.1279	**SHC 0.7: 0.1255**
	2	0°-8°	0.1069	I	-	SPSC: 0.0784	SSR$_C$C: 0.0749	SOC 0.5: 0.0744	**SSHC: 0.0710**
				P	SRC 0.3: 0.0735	SSC 0.7: 0.0793	SR$_C$C 0.7: 0.0734	**SOC 0.3: 0.0697**	SHC 0.7: 0.0712
	3	12°-16°	0.2985	I	-	**SPSC: 0.1750**	SPR$_C$C: 0.1791	SSOC: 0.1753	SPHC: 0.1869
				P	SRC 0.7: 0.2006	**SSSC: 0.1885**	SSR$_C$C: 0.2056	SOC 0.7: 0.2063	SSHC: 0.1997
	4	>14°	0.3124	I	-	SPSC: 0.2286	SPR$_C$C: 0.1954	**SSOC: 0.1793**	SHC 0.7: 0.2245
				P	SRC 0.5: 0.2770	**SPSC: 0.2582**	SSR$_C$C: 0.2643	SPOC: 0.2877	SHC 0.7: 0.2642
The best performance of average lift to drag coefficient	1	0°-16°	4.9473	I	-	**SSSC: 5.5721**	-	SOC 0.5: 5.0159	SHC 0.3: 4.9975
				P	-	-	-	-	-
	2	0°-8°	5.4311	I/P	-	-	-	-	-
	3	12°-16°	4.4636	I	-	**SSSC: 6.2270**	SSR$_C$C: 5.1202	SSOC: 4.8036	SPHC: 4.9884
				P	SRC 0.5: 4.6386	**SSSC: 4.7668**	SR$_C$C 0.3: 4.6483	SOC 0.7: 4.6848	SHC 0.7: 4.6574
	4	>14°	3.8331	I	-	**SSSC: 4.6153**	SPR$_C$C: 4.0887	SSOC: 4.2090	SPHC: 4.3428
				P	SRC 0.3: 3.9046	-	-	-	**SHC 0.7: 3.9555**

Note: The highlighted numbers in the table represent the best-performed cavity airfoil model at various regimes.

Regime 2
- SSHC(I) has reduced drag by 33.5%
- SOC(P) 0.3 has reduced drag by 34.7%

Regime 3
- SPSC(I) has reduced drag by 41.3% & SSSC(I) has improved (l/d) by 39.5%
- SSSC(P) has reduced drag by 36.8% & SSSC(P) has improved (l/d) by 6.7%

Regime 4
- SSOC(I) has reduced drag by 42.6% & SSSC(I) has improved (l/d) by 20.4%
- SPSC(P) has reduced drag by 17.3% & SHC(P) 0.7 has improved (l/d) by 3.1%

4.3 Output visualisation and overall discussion

Based on the individual study and regime wise comparative study, SOC(I) 0.5, SOC(P) 0.3, SSSC(I), and SSSC(P) models performed better compared to OA and other cavity models. Table 9 and Table 10 gives visualisation output based on these four different cavity airfoil models compared to OA. The visual results are compared at 16° AOA since the OA stalls before 16°. Since the output can't be visualised for all the 45 different models, better-performed models have been listed.

The coefficient of pressure (C_p) along the different airfoil models (SOC(I) 0.5, SOC(P) 0.3, SSSC(I), and SSSC(P)) at 10° AOA are plotted in Fig. 6. The C_p values are plotted along with the distance of leading edge to trailing edge (i.e.) the normalised axial distance. The maximum pressure difference occurs at the stagnation point, which shows a further divergence in the case of the cavity airfoil model.

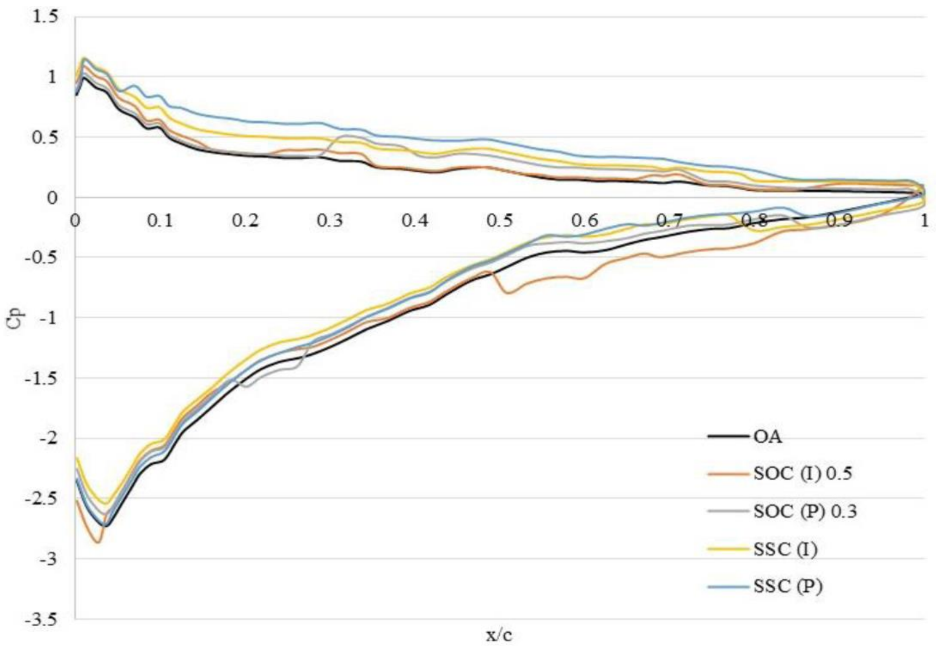

Fig. 6 C_p distribution along the x/c chord location at 10° AOA

As in Table 9, the OA shows higher pressure on the pressure side of the airfoil, which seems to be very low in all other cavity airfoil models. The low-pressure formation underneath the cavity airfoils is the main reason for lagging in lift generation. The formation of the boundary layer is visualised in velocity contouring Table 9. As in OA, the scattering of the boundary layer has occurred, which weakens the boundary layer flow, thereby results in flow detachment. In contrast, the cavity airfoil models do not scatter much boundary layer; hence the flow is kept energised.

As discussed in Table 10, it is visualised that there is an early detachment of streamlines in OA. In contrast, the cavity airfoil models show delayed detachment and even re-attachment of streamlines. Table 10 also shows the flow rendering, which differs according to boundary layer divergence. A maximum scattering of flow is observed in the original airfoil (OA). Cavity models show a reduction in the size of the wake formation with less vortex strength than the original airfoil. Considering the flow performance of the OA to that of chordwise attachment, the flow remains attached to the OA surface only up to 0.18C. In contrast, the cavity models show attached flow even

Table 9 Airfoil pressure and velocity contour @ 16° AOA

Airfoil model	Pressure contour @ 16° AOA	Velocity contour @ 16° AOA
OA	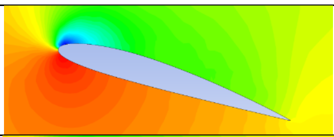	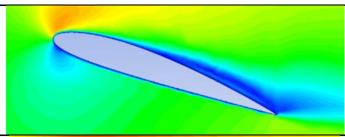
SOC (I) 0.5	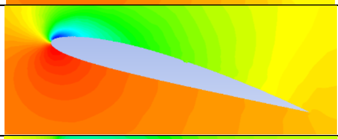	
SOC (P) 0.3	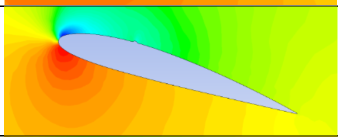	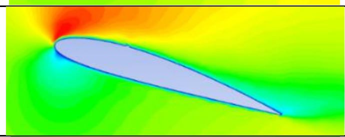
SSSC (I)	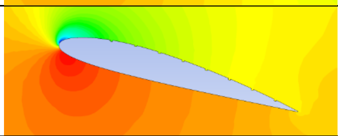	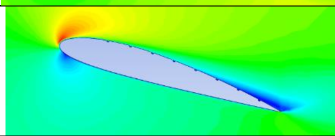
SSSC (P)	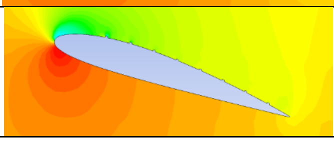	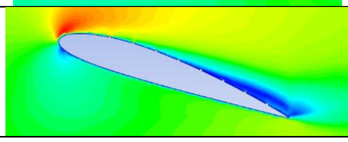

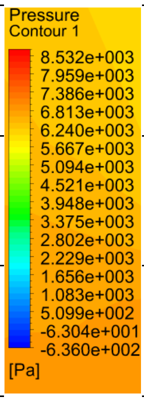

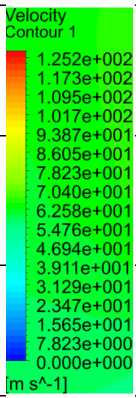

Table 10 Airfoil streamline pattern and flow rendering @ 16° AOA

Cavity model	Streamline comparison @ 16° AOA	Flow rendering @ 16° AOA
OA	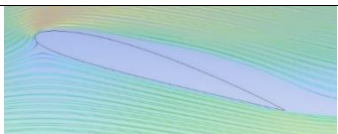	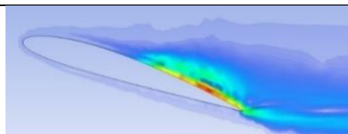
SOC (I) 0.5	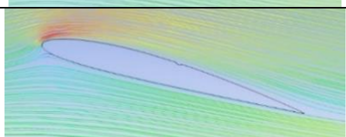	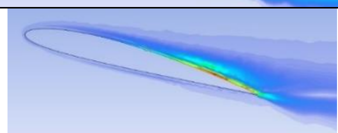
SOC (P) 0.3	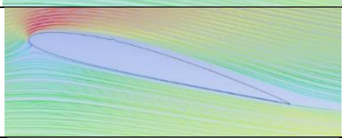	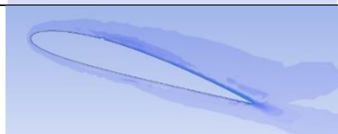
SSSC (I)	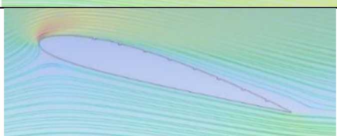	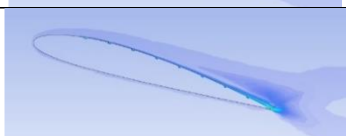
SSSC (P)	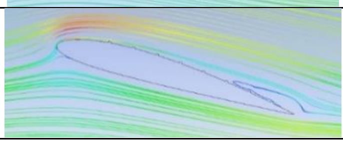	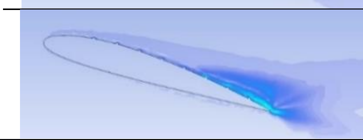

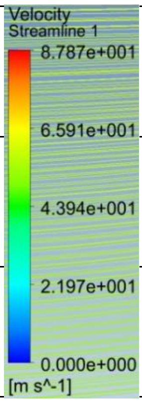

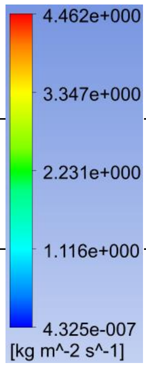

after 0.25C. Hence the stalling point is pushed forward. Thus, the results conclude that transition effect very differently depending on the AOA and surface cavity profile range.

5. Conclusions

This study presents the cavity effect over NACA 2412 airfoil at a velocity of 30 m/s with variable AOA (α=0° to 20°). For this purpose of study, RANS simulation with one equational commercial solver is employed. It has been proved that the cavity has a high impact on boundary layer transition with minimal adverse effects. Results clearly show that the aerodynamics coefficient of cavity airfoil significantly varies due to varied cavity geometry and orientation. In general, the suppression of the flow control technique showed a beneficial improvement on the cavity airfoil in the *l/d* ratio. In addition, the cavity airfoil shows the following potential benefits.

- The cavities over the surface improve flow behaviour. For example, roughness over a smooth surface has a proven result of decreasing drag and increasing lift to drag ratio by creating co-rotational flow within the cavity with improved flow behaviour.
- The aerodynamic characteristics show a leap in performance, especially placing the cavities at an adverse pressure gradient region.
- Pressure contour study shows that surface modifiers decrease the pressure drop.
- Cavity airfoil shows delayed boundary layer separation with less formation of vortices.
- The findings indicated that at higher AOA, streamlines recirculate due to the increase in wake formation with an adverse boundary layer development over the modified surface compared to the smooth surface.
- Postponed stalling characteristics.
- The complete analysis shows that flow re-attachment near the LE has a greater potential influence towards turbulence diffusion of linear momentum.

This numerical study improved the aerodynamic performance of the airfoil characteristics. Thus, the designed cavity airfoil model has successfully shown a better outcome.

Acknowledgments

This research was funded by Universiti Sains Malaysia Grant No. 1001/PAERO/8014120 and the APC was funded by Universiti Sains Malaysia. The authors confirm that the data supporting the findings of this study are available within the article. The authors declare no conflict of interest.

References

Afzal, A., Aabid, A., Khan, A., Afghan Khan, S., Rajak, U., Nath Verma, T. and Kumar, R. (2020), "Response surface analysis, clustering, and random forest regression of pressure in suddenly expanded high-speed aerodynamic flows", *Aerosp. Sci. Technol.*, **107**, 106318. https://doi.org/10.1016/j.ast.2020.106318.

Afzal, A., Khan, S.A., Islam, M.T., Jilte, R.D., Khan, A. and Soudagar, M.E.M. (2020), "Investigation and back-propagation modeling of base pressure at sonic and supersonic Mach numbers", *Phys. Fluid.*, **32**(9), 096109. https://doi.org/10.1063/5.0022015.

Al-Jibory, M.W. and Shinan, H.A.A. (2020), "Numerical study of the boundary layer separation control on the NACA 0012 airfoil using triangular rib", *IOP Conf. Ser.: Mater. Sci. Eng.*, **671**(1), 012144.

Al-Obaidi, A.S. and Pei Soh, Z. (2016), “Numerical analysis of the shape of dimple on the aerodynamic efficiency of NACA 0012 airfoil”, *International Grand Challenges Engineering Research Conference (6th eureca)*, Kuala Lumpur, Malaysia.

Aldheeb, M., Asrar, W., Omar, A., Altaf, A. and Sulaeman, E. (2020), “Effect of a directionally porous wing tip on tip vortex”, *J. Appl. Fluid Mech*., **13**(2), 651-665. https://doi.org/10.29252/JAFM.13.02.29738.

Arunraj, R., Logesh, K., Balaji, V., Ravichandran, T. and Yuvashree, G. (2019), “Experimental investigation of lift enhancement by suction-assisted delayed separation of the boundary layer on NACA 0012 airfoil”, *Int. J. Ambient Energy*, **40**(3), 243-247. https://doi.org/10.1080/01430750.2017.1386127.

Beves, C.C. and Barber, T.J. (2017), “The wingtip vortex of a dimpled wing with an endplate”, *J. Fluid. Eng*., **139**(2), 021202. https://doi.org/10.1115/1.4034525.

Chakroun, W., Al-Mesri, I. and Al-Fahad, S. (2004), “Effect of surface roughness on the aerodynamic characteristics of a symmetrical airfoil”, *Wind Eng*., **28**(5), 547-564. https://doi.org/10.1260/0309524043028136.

Chang, P.K. (1970), *CHAPTER I - Introduction to the Problems of Flow Separation*, Pergamon.

Chang, P.K. (2014), *Separation of Flow*, Elsevier.

D’Alessandro, V., Clementi, G., Giammichele, L. and Ricci, R. (2019), “Assessment of the dimples as passive boundary layer control technique for laminar airfoils operating at wind turbine blades root region typical reynolds numbers”, *Energy*, **170** 102-111. https://doi.org/10.1016/j.energy.2018.12.070.

Dandan, M.A., Samion, S., Musa, M.N. and Zawawi, F.M. (2019), “Evaluation of lift and drag force of outward dimple cylinder using wind tunnel”, *CFD Lett*., **11**(3), 145-153.

Eleni, D.C., Athanasios, T.I. and Dionissios, M.P. (2012), “Evaluation of the turbulence models for the simulation of the flow over a national advisory committee for aeronautics (NACA) 0012 airfoil”, *J. Mech. Eng. Res*., **4**(3), 100-111. https://doi.org/10.5897/JMER11.074.

Faruqui, S.H.A., AlBari, M.A. and MdEmran, A.F. (2014), “Numerical analysis of role of bumpy surface to control the flow separation of an airfoil”, *Procedia Eng*., **90** 255-260. https://doi.org/10.1016/j.proeng.2014.11.846.

Feng, L.H., Choi, K.S. and Wang, J.J. (2015), “Flow control over an airfoil using virtual gurney flaps”, *J. Fluid Mech*., **767** 595-626. https://doi.org/10.1017/jfm.2015.22.

Hoffmann, K.A. and Chiang, S.T. (2000), *Computational Fluid Dynamics Volume I*, Engineering Education System.

Lake, J., King, P. and Rivir, R. (2000), “Low reynolds number loss reduction on turbine blades with dimples and V-grooves”, *38th Aerospace Sciences Meeting And Exhibit*.

Lin, J., Robinson, S., Mcghee, R. and Valarezo, W. (1992), “Separation control on high reynolds number multi-element airfoils”, *10th Applied Aerodynamics conference*, Palo Alto, CA, June.

Livya, E., Anitha, G. and Valli, P. (2015), “Aerodynamic analysis of dimple effect on aircraft wing”, *Int. J. Mech. Aerosp. Indus. Mechatron. Manuf. Eng*., **9**(2), 350-353.

Lopes, A. (2016), “A 2D software system for expedite analysis of CFD problems in complex geometries”, *Comput. Appl. Eng. Edu*., **24**(1), 27-38. https://doi.org/10.1002/cae.21668.

Manni, L., Nishino, T. and Delafin, P.L. (2016), “Numerical study of airfoil stall cells using a very wide computational domain”, *Comput. Fluid*., **140**, 260-269. https://doi.org/10.1016/j.compfluid.2016.09.023.

Matsson, J.E., Voth, J.A., McCain, C.A. and McGraw, C. (2016), “Aerodynamic performance of the NACA 2412 airfoil at low reynolds number”, *2016 ASEE Annual Conference & Exposition*, New Orleans, Louisiana, June.

Merryisha, S. and Parvathy, R. (2019), “Experimental and CFD analysis survey of surface modifiers on aircraft wing”, *J. Adv. Res. Fluid Mech. Therm. Sci.*, **11**(10), 46-56.

Merryisha, S. and Rajendran, P. (2019), “Aircraft wing aerodynamic efficiency improvement using longitudinal spanwise grooves”, *AEROMECH 2019*, The Light, Pulau Pinang, Malaysia, November.

Merryisha, S. and Rajendran, P. (2019), “A review of winglets on tip vortex, drag and airfoil geometry”, *J. Adv. Res. Fluid Mech. Therm. Sci*., **63**(2), 218-237.

Mueller, T.J. and DeLaurier, J.D. (2003), “Aerodynamics of small vehicles”, *Ann. Rev. Fluid Mech*., **35**(1), 89-111. https://doi.org/10.1146/annurev.fluid.35.101101.161102.

Rajasai, B., Tej, R. and Srinath, S. (2015), "Aerodynamic effects of dimples on aircraft wing", *Int. J. Adv. Mech. Aeronaut. Eng*., **2**(2), 169-172.

Ramprasadh, C. and Devanandh, V. (2015), "A CFD study on leading edge wing surface modification of a low aspect ratio flying wing to improve lift performance", *Int. J. Micro Air Vehic*., **7**(3), 361-373. https://doi.org/10.1260/1756-8293.7.3.361.

Saraf, A.K., Singh, M.P. and Chouhan, T.S. (2017), "Effect of dimple on aerodynamic behaviour of airfoil", *Int. J. Eng. Technol*., **9**(3), 2268-2277.

Schubauer, G.B. and Spangenberg, W. (1960), "Forced mixing in boundary layers", *J. Fluid Mech*., **8**(1), 10-32. https://doi.org/10.1017/S0022112060000372.

Srivastav, D. (2012), "Flow control over airfoils using different shaped dimples", *International Conference on Fluid Dynamics and Thermodynamics Technologies*, March.

Venkatesan, S., Kumar, V.P., Kumar, M.S. and Kumar, S. (2018), "Computational analysis of aerosynamic characterists of dimple airfoil NACA 2412 at various angle of attack", *Int. J. Mech. Eng. Technol*., **9**(9), 41-49.

Wang, X.Y., Lee, S., Kim, P. and Seok, J. (2015), "Aerodynamic effect of 3D pattern on airfoil", *Tran. Can. Soc. Mech. Eng*., **39**(3), 537-545. https://doi.org/10.1139/tcsme-2015-0041.

Zhang, P., Rao, Y. and Li, Y. (2018), "A numerical study of heat transfer and flow structure in channels with miniature V rib-dimple hybrid structure on one wall", *ASME Turbo Expo 2018: Turbomachinery Technical Conference and Exposition*, Oslo, Norway, June.

GY